Thin Solid Films 520 (2012) 5946–5951

Contents lists available at SciVerse ScienceDirect

Thin Solid Films

journal homepage: www.elsevier.com/locate/tsf

Optimized inductively coupled plasma etching for poly(methyl-methacrylate-glycidly-methacrylate) optical waveguide

Xiaoqiang Sun [a,b], Xiaodong Li [b], Changming Chen [b], Kun Zhang [b], Jie Meng [b], Xibin Wang [b], Tianfu Yang [b], Daming Zhang [b], Fei Wang [b], Zhiyuan Xie [a,*]

[a] Changchun Institute of Applied Chemistry, Chinese Academy of Sciences, No. 5625, Renming Street, Changchun, Jilin 130022, China
[b] State Key Laboratory on Integrated Optoelectronics, Jilin University, Changchun, Jilin 130012, China

ARTICLE INFO

Article history:
Received 7 July 2011
Received in revised form 5 May 2012
Accepted 10 May 2012
Available online 16 May 2012

Keywords:
Inductively coupled plasma
Etching
Polymers
Optical waveguides
Scanning electron microscopy
Atomic force microscopy

ABSTRACT

Optical loss is a crucial quality for the application of polymer waveguide devices. The optimized oxygen inductively coupled plasma etching conditions, including antenna power, bias power, chamber pressure, O_2 flow rate and etching time for the fabrication of smooth vertical poly(methyl-methacrylate-glycidly-methacrylate) channel waveguide were systematically investigated. Atomic force microscopy and scanning electron microscopy were used to characterize the etch rate, surface roughness and vertical profiles. The increment of etch rate with the antenna power, bias power and O_2 flow rate was observed. Bias power and chamber pressure were found to be the main factor affecting the interface roughness. The vertical profiles were proved to be closely related to antenna power, bias power and O_2 flow rate. Surface roughness increment was observed when the etching time increased.

© 2012 Elsevier B.V. All rights reserved.

1. Introduction

Polymeric waveguide components are promising alternatives for the application of optical interconnects [1,2], wavelength division multiplex [3], and sensors [4] due to the merits of low optical loss, controllable refractive index, easy fabrication and good chemical stability [5,6]. Conventional semiconductor processing technologies, such as spin-coating, photolithography and etching can be used in the fabrication of polymer waveguides [6,7]. As a widely used technique, plasma etching is reported to be an effective method to form good waveguide morphology [8,9]. However, the roughness at interface is an unfavorable consequence of plasma etching. This roughness may induce significant waveguide scattering loss and severely impede scaling down of waveguide dimensions [10,11]. Thus, the interface roughness needs to be well studied and understood. It is well known that both isotropic chemical etching and anisotropic ionic bombardment exist in plasma-etching process. Many efforts have been devoted to study the roughness evolution during etching, and optimize the etching conditions to obtain smooth vertical profiles to reduce optical loss due to scattering [12–15].

Oxygen-based reactive ion etching (RIE) is a well established process for polymer waveguide fabrication [16,17]. However, the ion density and energy cannot be regulated individually in the RIE process. They are both controlled by one radio-frequency (RF) power. Though high RF power accelerates the etching process, it may induce serious ions sputtering and damage the film surface. Different from RIE method, inductively coupled plasma (ICP) etching adopts a secondary RF power to generate high-density plasmas ($>10^{11}$ cm^{-3}), which is more suitable for submicron and uniform process. This plasma source is independent of plasma energy that is controlled by another bias power source [18]. Thus, ICP etching can provide smoother interface, higher etch rate and vertical figure for polymer devices than RIE approach [19]. Previous work has published some experimental results about oxygen ICP etching with polymers. It just focused on a few aspects of ICP etching, such as antenna power or etching chamber pressure. The research of different factors affecting etching results still needs to be done, especially for those commonly used materials.

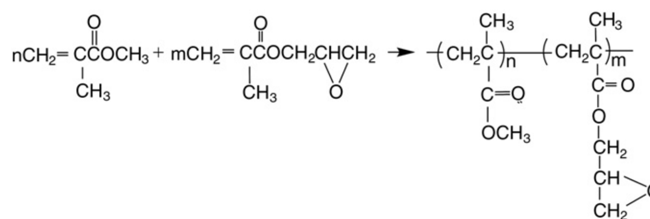

Fig. 1. Molecular structure of P(MMA-GMA).

* Corresponding author. Tel.: +86 431 852 628 19; fax +86 431 856 849 37.
E-mail address: xiezy_n@ciac.jl.cn (Z. Xie).

0040-6090/$ – see front matter © 2012 Elsevier B.V. All rights reserved.
doi:10.1016/j.tsf.2012.05.016

www.spm.com.cn

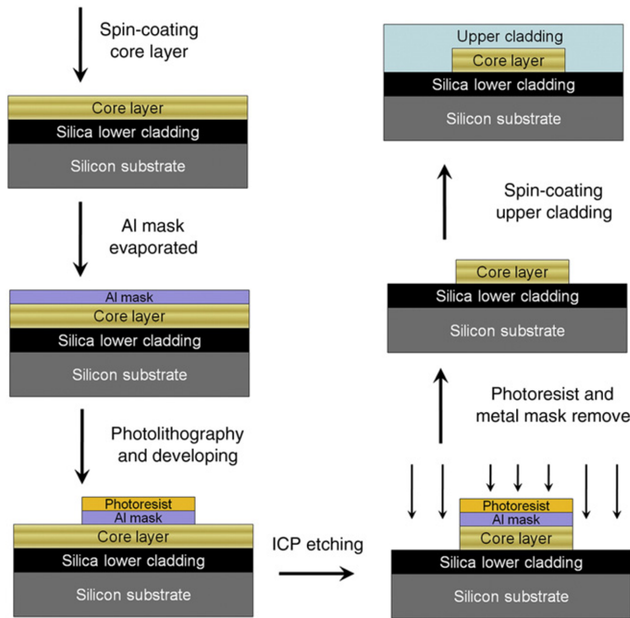

Fig. 2. Process flow for the fabrication of channel waveguide using ICP etching.

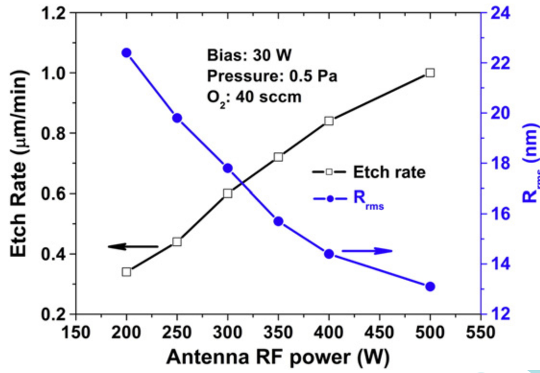

Fig. 3. Etch rate and R_{rms} as a function of antenna RF power at 30 W bias RF power, 40 sccm O_2 flow rate and 0.5 Pa chamber pressure.

In this study, the etch rate, surface roughness and vertical profiles were evaluated as a function of antenna RF power, bias RF power, chamber pressure and O_2 flow rate for poly(methyl-methacrylate-glycidly-methacrylate) (P(MMA-GMA)) channel waveguide fabrication.

2. Experimental details

2.1. Materials

P(MMA-GMA) material synthesized by ourselves was used in this study due to its desirable characteristics [20]. The molecular structure of P(MMA-GMA) is shown in Fig. 1. It can be used for arrayed waveguide gratings (AWGs), optical switches, modulators, and other optical devices. The refractive index (RI) of P(MMA-GMA) was measured to be 1.48 at 1550 nm. Bisphenol-A epoxy was adopted as the RI regulator in P(MMA-GMA) to form the core material. The root-mean-square roughness (R_{rms}) of P(MMA-GMA) film was 0.32 nm for an area of 20 μm^2.

2.2. Channel waveguide

A channel waveguide was used to study the optimization of oxygen ICP etching conditions. Fig. 2 presents the schematic diagram of fabrication process. Firstly, P(MMA-GMA) was spin-coated onto the silica lower cladding on a silicon substrate at 2500 rpm. After a subsequent bake at 120 °C for 2.5 h, a layer of 100 nm thick aluminum film was thermal evaporated onto the top of P(MMA-GMA) film as the metal mask. To define the waveguide patterns on Al film, BP212 photoresist was spin-coated and patterned by traditional photolithography [7]. No significant sawteeth were observed at the edge of Al etch mask. The oxygen ICP etching process was performed for 150 s under different conditions in a 13.56 MHz CE-300I (ULVAC Co. Inc, Japan) etching machine. A He-cooling system was used to control the bottom electrode temperature. To obtain smooth vertical optical waveguides, the etching parameters were optimized under the condition that one parameter was changed while the other parameters were fixed [21,22]. Atomic force microscopy (AFM) images were recorded with a multimode scanning probe microscope CSPM5000 that operated in contact mode (Being Nano-Instrument Ltd., China). The tip of Contact-G was used for AFM measurements (Innovative Solutions

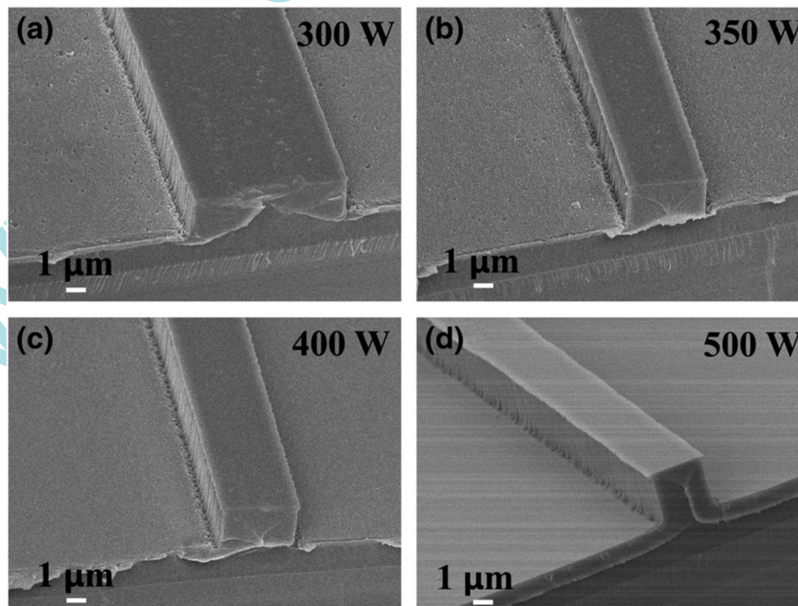

Fig. 4. SEM images of P(MMA-GMA) waveguide vertical profiles when antenna RF power is set to (a) 300 W, (b) 350 W, (c) 400 W, (d) 500 W, at 30 W bias RF power, 40 sccm O_2 flow rate, and 0.5 Pa chamber pressure.

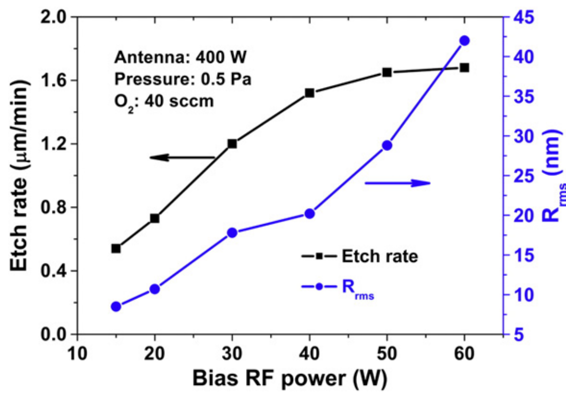

Fig. 5. Etch rate and R_{rms} as a function of bias RF power at 400 W bias RF power, 40 sccm O_2 flow rate and 0.5 Pa chamber pressure.

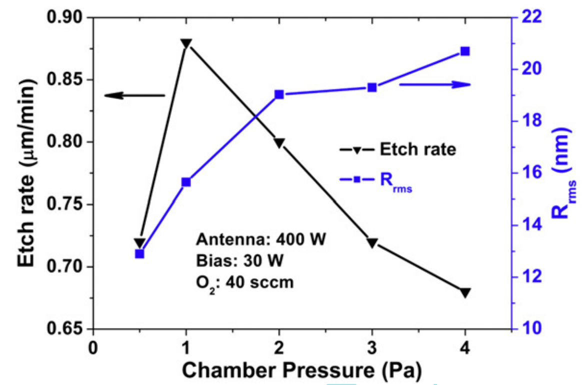

Fig. 7. Etch rate and surface roughness as a function of chamber pressure at 400 W antenna RF power, 30 W bias RF power and 40 sccm O_2 flow rate.

Bulgaria Ltd., Bulgaria). The morphological characterization of the waveguide was examined by means of scanning electron microscopy (SEM) JSM-7600F (JEOL Ltd., Japan) that operated on a voltage of 5 kV.

3. Results and discussion

3.1. The effect of antenna RF power

Firstly, the effect of antenna RF power on the etch rate, surface roughness and vertical profiles of P(MMA-GMA) waveguide was investigated [8,9]. The antenna RF power was varied from 200 to 500 W when the other parameters were fixed at 30 W bias RF power, 0.5 Pa chamber pressure, and 40 sccm O_2 flow rate.

The etch rate and surface roughness as a function of antenna RF power are shown in Fig. 3. When the antenna RF power increased from 200 to 500 W, the etch rate increased from 0.34 to 1.00 μm/min. This phenomenon can explain that the antenna RF power plays a major role for dissociating oxygen molecules into reactive radicals and ionic species, and then the plasma density. Chemical etching was enhanced with this improved antenna RF power and plasma density. As a consequence, R_{rms} of the polymer film decreased from 22.4 to 13.1 nm.

Fig. 4 shows the SEM images of channel waveguide vertical profiles after performing ICP etching under different antenna RF powers. The sidewall roughness was less than 50 nm at all conditions and decreased with the increment of antenna RF power. Vertical edge, which is a key issue for constraining mode light field and reducing optical loss, was observed when the antenna RF power was increased to 400 W, as shown in Fig. 4(c). The channel waveguide showed trapezoidal under powers below 400 W, as shown in Fig. 4(a) and (b). Besides, 500 W antenna RF power led to an undercut phenomenon and the overhang of metal mask above the channel waveguide because of the isotropic etching caused by the increased plasma density [12,13], as shown in Fig. 4(d). Thus, 400 W antenna RF power is a moderate choice to obtain smooth vertical profiles.

3.2. The effect of bias RF power

To evaluate the effect of bias RF power on the etch rate, surface roughness and vertical profiles of P(MMA-GMA) waveguide, bias RF power were increased from 15 to 60 W when the other parameters were fixed at 400 W antenna RF power, 0.5 Pa chamber pressure,

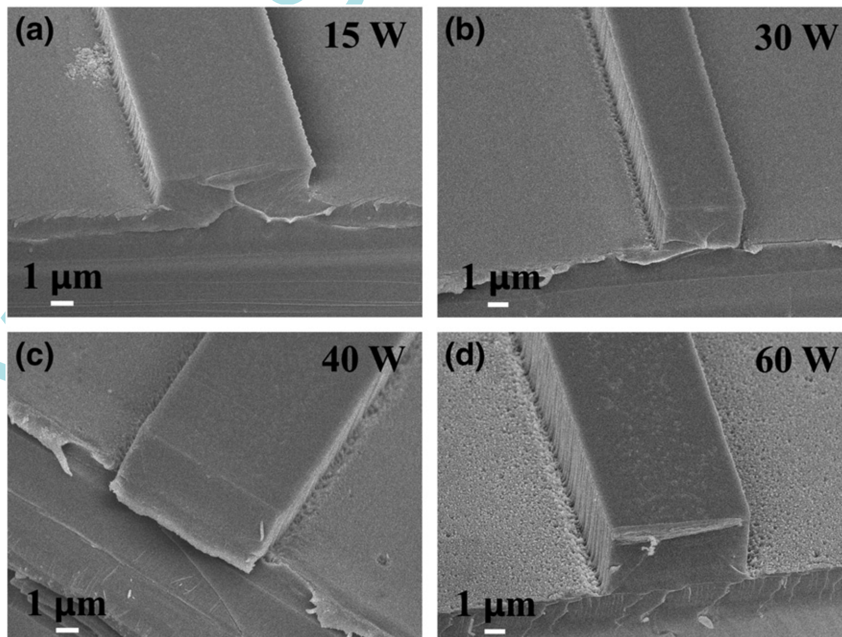

Fig. 6. SEM images of P(MMA-GMA) channel waveguide after ICP etching when bias RF power is set to (a) 15 W, (b) 30 W, (c) 40 W, (d) 60 W, at 400 W antenna RF power, 40 sccm O_2 flow rate, and 0.5 Pa pressure.

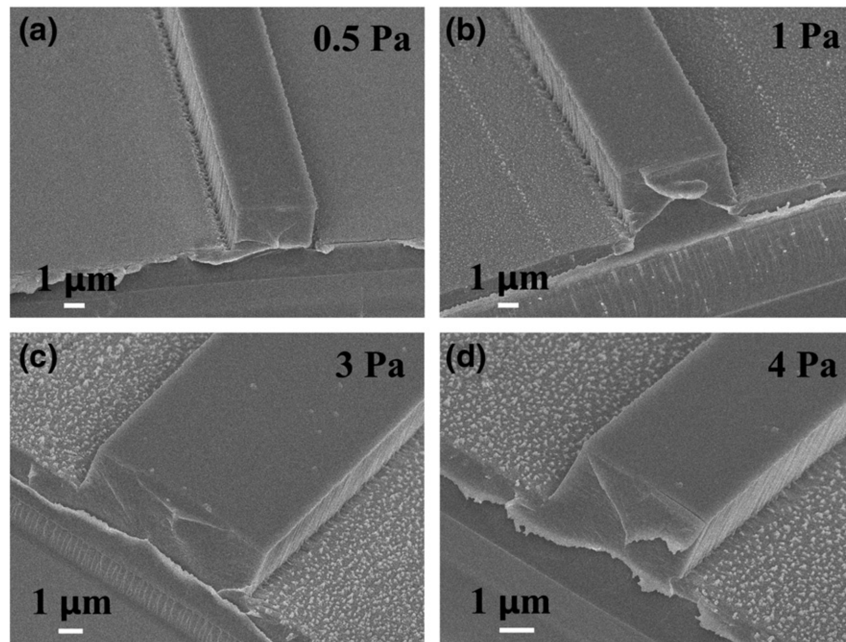

Fig. 8. SEM images of P(MMA-GMA) channel waveguide at 400 W antenna RF power, 40 W bias RF power, 40 sccm O_2 flow rate, and chamber pressure of (a) 0.5 Pa, (b) 1 Pa, (c) 3 Pa, (d) 4 Pa.

and 40 sccm O_2 flow rate. As shown in Fig. 5, the etch rate increases from 0.54 to 1.68 μm/min. It is well known that the plasma energy is mainly determined by the bias RF power and controls the directional movement of plasmas in ICP etching [23]. Since the etch rate increased nearly three times within a narrow power increment of 45 W, the bias RF power was proved to be a key issue affecting the etch rate. As is clear in Fig. 5, R_{rms} significantly increased from 8.5 to 42 nm when the bias RF power changed from 15 to 60 W. It indicates that the surface roughness strongly depends on the plasma bombardment and is enhanced with the increment of bias RF power [24].

Fig. 6 shows the SEM images of cross-sectional waveguide scheme after ICP etching. The expected smoother surface at 15 W is clearly illustrated in Fig. 6(a). However, the directionality of plasma movement was weakened and the chemical reaction induced isotropic etching predominated over anisotropic etching at this small bias power. It led to the undesired undercut [25]. The best vertical edge was observed at 30 W bias RF power, as shown in Fig. 6(b). The sidewall vertical angle was less than 2° when 30 W bias RF power was applied. Considering the appearance of increased interface roughness in Fig. 6(c) and (d), 30 W bias RF power is more preferable to obtain the smooth vertical waveguide.

3.3. The effect of chamber pressure

The effect of chamber pressure on the etch rate and surface roughness was investigated when the other parameters were fixed at 400 W antenna RF power, 30 W bias RF power and 40 sccm O_2 flow rate. As shown in Fig. 7, the etch rate increased from 0.72 to 0.88 μm/min as the chamber pressure increased from 0.5 to 1 Pa and reduced to 0.68 μm/min when the chamber pressure increased from 1 to 4 Pa. A peak value of etch rate was found in the process of chamber pressure increasing. It can be explained that the gas molecules and dissociated plasmas were increasing when the chamber pressure was lower than 1 Pa. The etch rate and the plasma etching were enhanced. However, further reactive species increasing was limited by the fixed antenna RF power when the chamber pressure was over 1 Pa. Besides, the kinetic energy of plasmas reduced for the shortened mean free path. This explains the etch rate falling at pressures over 1 Pa.

As shown in Fig. 7, when the chamber pressure changed from 0.5 to 4 Pa, the roughness increased from 12.9 to 20.7 nm. Agarwal et al. have reported that the distance between the collisions of plasmas is closely related to the incident angles of oxygen etchant [17]. Thus, the roughness variation observed can be explained by the influence of oxygen plasma incident angles on the film surface and the subsequent redistribution of oxygen gas flow due to local morphological features. This mechanism means if no reaction happens on the first hit between the oxygen plasma and the P(MMA-GMA) film, the reactant reflects toward valleys on the film surface. It leads to more partial etching of hollows contrasting with peaks [13,18]. Thus, oxygen plasmas are incident at larger oblique angles, which results in smoother surface at the lower pressure of 1 Pa. This oxygen plasma redistribution pattern explains the roughness evolution observed from the etching results.

Vertical profiles after plasma etching at different chamber pressures are clearly illustrated by SEM images in Fig. 8. According to the above analysis, plasmas were incident at normal angles on the waveguide sidewall at higher pressures, which resulted in trapezoidal figures, as shown in Fig. 8(c) and (d). However, the plasmas flux was nearly vertically incident on the substrate at pressures of 0.5 and 1 Pa, as shown in Fig. 8(a) and (b). Considering the roughness

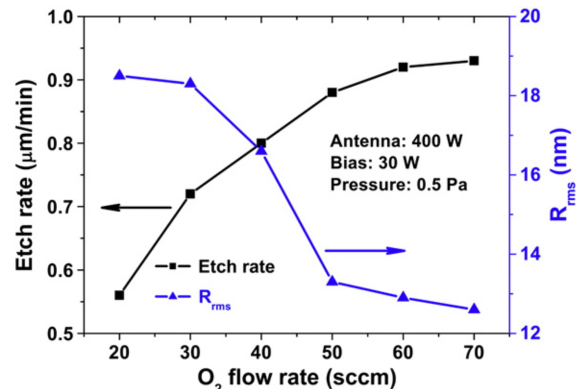

Fig. 9. Etch rate and surface roughness as a function of O_2 flow rate at 0.5 Pa chamber pressure, 400 W antenna RF power and 30 W bias RF power.

www.spm.com.cn

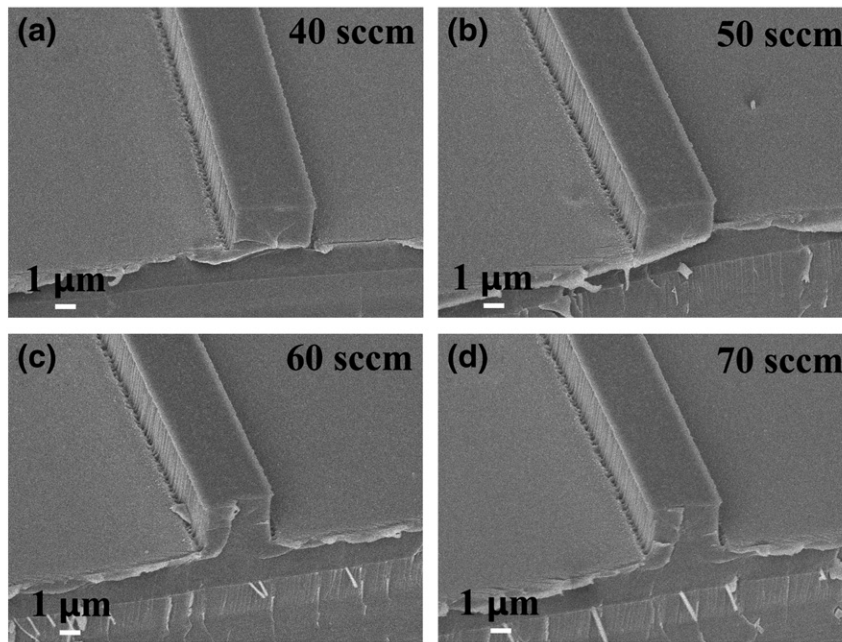

Fig. 10. SEM images of P(MMA-GMA) channel waveguide at 400 W antenna RF power, 40 W bias RF power, 0.5 Pa chamber pressures and O_2 flow rate of (a) 40 sccm, (b) 50 sccm, (c) 60 sccm, (d) 70 sccm.

condition, a chamber pressure of 0.5 Pa is preferable to obtain smoother vertical profiles.

3.4. The effect of O_2 flow rate

The effect of O_2 flow rate on the etch rate and surface roughness was investigated, too. It was changed from 20 to 60 sccm when the other parameters were fixed at 400 W antenna RF power, 30 W bias RF power, and 0.5 Pa chamber pressure. The variation of the etch rate and surface roughness as a function of O_2 flow rate is shown in Fig. 9. The etch rate increased from 0.56 to 0.93 μm/min when the flow rate increased from 20 to 70 sccm. This can be explained that the plasma density and chemical etching effect are enhanced with the increment of O_2 flow rate. This increment reduces the mean free path and the directional movement of oxygen plasmas. Thus, further increasing flow rate cannot accelerate the removal of substrate by the reaction of reactive species and polymer molecules significantly [25,26]. Consequently, the etch rate became saturating when the O_2 flow rate was over 40 sccm, and R_{rms} decreased from 18.5 to 12.6 nm when the flow rate increased from 20 to 70 sccm, as shown in Fig. 9.

Vertical profiles of the channel waveguide after plasma etching at different O_2 flow rates are clearly illustrated by SEM images in Fig. 10. No significant flow rate induced sidewall roughness variation is observed in the figure. However, an undercut phenomenon that results from the weakness of anisotropic etching accompanied with plasma density increasing appears as the O_2 flow rate reaches 50 sccm, as shown in Fig. 10(b). Besides, the waveguide height does not change appreciably when the etch rate increases from 60 to 70 sccm, as shown in Fig. 10(c) and (d). Thus, the etch rate has saturated at 60 sccm. As a result, the flow rate of 40 sccm is more preferable to fabricate the smooth vertical waveguide. An etch rate of 0.8 μm/min and R_{rms} of 16.6 nm are obtained at 400 W antenna RF power, 30 W bias RF power, 0.5 Pa chamber pressure, and 40 sccm O_2 flow rate.

3.5. The effect of etching time

According to the working principles of ICP etching and previous work, surface roughness is not independent of etching time [19,27]. So, the effect of etching time on the surface roughness of P(MMA-GMA) was investigated while the antenna RF power, bias RF power, chamber pressure, and O_2 flow rate were set to be 300 W, 30 W, 0.5 Pa, and 40 sccm, respectively. The R_{rms} of blank P(MMA-GMA) films as a function of the etching time is shown in Fig. 11. Since the surface roughness induced by bombard effect is inherited from the previous etching, R_{rms} increased four times when the etching time ranged from 3 to 6 min. Moreover, longer etching time can cause extra heat on the bottom electrode. Though the ICP system has an excellent cooling chuck, the accumulated heat in the silicon substrate may bring unfavorable impacts to the film surface. Thus, a shorter etching time or faster etch rate is more desirable to obtain preferable film surface.

According to the above parameter evaluations, smooth surface and sidewall arise mainly from the conflicting effects between the chemical etching and ion bombardment. Except for ICP etching parameters, the depositions on the internal wall of chamber can affect the collision, absorption and compound of plasmas, and then influence the stability and efficiency of etching process. Thus, a clean chamber condition is essential for performing a repeatable and uniform ICP etching [28].

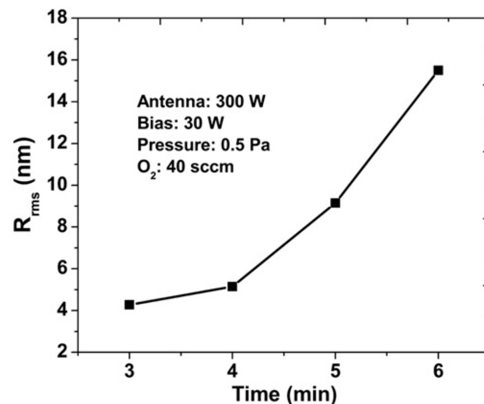

Fig. 11. Surface roughness as a function of the etching time.

www.spm.com.cn

4. Conclusion

This study presented relatively complete and systematic research on the polymer waveguide ICP etching conditions, especially those affected sidewall figures. The optimized oxygen ICP etching parameters of P(MMA-GMA) film with Al metal mask were characterized in detail. The increment of etch rate with the antenna RF power, bias RF power and O_2 flow rate was observed. Bias power was found to be the main factor for the surface and sidewall roughness. Vertical profiles were proved to be closely related to the antenna RF power, bias RF power and O_2 flow rate. Longer etching time led to larger surface roughness. A channel waveguide with smooth vertical sidewall was obtained under 400 W antenna RF power, 30 W bias RF power, 0.5 Pa chamber pressure, and 40 sccm O_2 flow rate. An etch rate of 0.8 μm/min and R_{rms} of 16.6 nm were obtained at the above parameters. As a typical process, the oxygen plasma etching of classic epoxy polymer P(MMA-GMA) shares the same mechanism and rules with those polymers that possess similar chemical and physical characteristics. Therefore, we believe the summarized conclusions are useful for the fabrication of polymer optical waveguides.

Acknowledgments

This work was supported by the National Natural Science Foundation of China (under grant nos 61107019, 61077041, 61177027 and 60807029), the Program for Special Funds of Basic Science & Technology of Jilin University (under grant nos 201103071, 201100253 and 200905005), the Science Foundation for Young Scientists of Jilin Province (no 20100174) and the Science and Technology Development Plan of Jilin Province (no 20110315).

References

[1] N. Bamiedakis, J. Beals, R.V. Penty, I.H. White, J.V. DeGroot, T.V. Clapp, IEEE J. Quant. Electron. 45 (2009) 415.
[2] M. Fujiwara, Y. Shirato, H. Owari, K. Watanabe, M. Matsuyama, K. Takahama, T. Mori, K. Miyao, K. Choki, T. Fukushima, T. Tanaka, M. Koyanagi, 6th International Conference on Polymers and Adhesives in Microelectronics and Photonics, Tokyo, Japan, IEEE Conference Proceedings, January 16–18 2007, p. 193.
[3] F. Wang, C.S. Ma, W. Sun, A. Li, Y. Zhao, H.M. Zhang, Z.H. Jiang, D.M. Zhang, Microw. Opt. Technol. Lett. 42 (2004) 192.
[4] M. Cheng, J. Hiltunen, M. Wang, A. Suutala, P. Karioja, R. Myllyla, Proc. Conference on Laser Applications in Life Sciences, Oulu, Finland, JUN 09–11, SPIE 7376, 2010, p. 73761A.
[5] L. Eldada, L.W. Shacklette, IEEE J. Sel. Top. Quant. 6 (2000) 54.
[6] W.N. Herman, W.Y. Chen, Y. Kim, G. Hutchinson, W.L. Cao, Y.Z. Leng, V. Yun, H.Y. Liang, Y.H. Peng, M. Du, L. Lucas, P.T. Ho, J. Goldhar, C.H. Lee, in: Robert A. Norwood, Manfred Eich, Mark G. Kuzyk (Eds.), Linear and Nonlinear Optics of Organic Materials IV, Denver, U.S.A., August 2–3, SPIE 5517, 2004, p. 1.
[7] Y. Zhao, D.M. Zhang, F. Wang, Z.C. Cui, M.B. Yi, C.S. Ma, W.B. Guo, S.Y. Liu, Opt. Laser Technol. 36 (2004) 657.
[8] W.M. Diffey, R.H. Trimm, M.G. Temmen, P.R. Ashley, IEEE J. Lightwave Technol. 23 (2005) 1787.
[9] J.W. Kang, J.S. Kim, J.J. Kim, Jpn. J. Appl. Phys. 40 (2001) 3215.
[10] M.H. Ibrahim, N.M. Kassim, A.B. Mohammad, A.S.M. Supa'at, Optoelectron. Adv. Mater. 3 (2009) 917.
[11] Y.J. Wang, Z.L. Lin, X.L. Cheng, C.S. Zhang, F. Gao, F. Zhang, Appl. Phys. Lett. 85 (2004) 3995.
[12] B. Schuppert, E. Brose, K. Petermann, R. Moosburger, J. Vac. Sci. Technol., A 18 (2000) 385.
[13] J.H. Kim, E.J. Kim, H.C. Choi, C.W. Kim, J.H. Cho, Y.W. Lee, B.G. You, S.Y. Yi, H.J. Lee, K. Han, W.H. Jang, T.H. Rhee, J.W. Lee, S.J. Pearton, Thin Solid Films 341 (1999) 192.
[14] S. Tachia, J. Vac. Sci. Technol., A 21 (2003) S131.
[15] G.S. Oehrlein, R.J. Phaneuf, D.B. Graves, J. Vac. Sci. Technol. B 29 (2011) 010801.
[16] Y. Zhao, F. Wang, Z.C. Cui, J. Zheng, H.M. Zhang, D.M. Zhang, S.Y. Liu, M.B. Yi, Microelectron. J. 35 (2004) 605.
[17] N. Agarwal, S. Ponoth, J. Plawsky, P.D. Persans, J. Vac. Sci. Technol., A 20 (2002) 1587.
[18] G. Schiller, M. Muller, F. Gitzhofer, J. Therm. Spray Techn. 8 (1999) 389.
[19] John H. Keller, John C. Forster, Michael S. Barnes, J. Vac. Sci. Technol., A 11 (1993) 2487.
[20] X. Fei, N. Fu, Y. Wang, J. Hu, Z.C. Cui, D.M. Zhang, C.X. Ma, S.Y. Liu, B. Yang, Chem. J. Chinese U. 27 (2006) 571.
[21] T. Ono, T. Akagi, T. Ichiki, J. Appl. Phys. 105 (2009) 013314.
[22] S.J. Pearton, D.R. Norton, Plasma Process. Polym. 2 (2005) 16.
[23] H.C. Lee, J.Y. Bang, C.W. Chung, Thin Solid Films 519 (2011) 7009.
[24] H.C. Lee, M.H. Lee, C.W. Chung, Appl. Phys. Lett. 96 (2010) 071501.
[25] T. Standaert, P.J. Matsuo, X. Li, G.S. Oehrlein, T.M. Lu, R. Gutmann, C.T. Rosenmayer, J.W. Bartz, J.G. Langan, W.R. Entley, J. Vac. Sci. Technol., A 19 (2001) 435.
[26] N. Rahmanian, S. Kim, G.P. Nordin, J. Vac. Sci. Technol. B 24 (2006) 2672.
[27] H. Kim, S.J. Jung, Y.H. Han, H.Y. Lee, J.N. Kim, D.S. Jang, J.J. Lee, Thin Solid Films 516 (2008) 3530.
[28] G. Cunge, B. Pelissier, O. Joubert, R. Ramos, C. Maurice, Plasma Sources Sci. Technol. 14 (2005) 599.

www.spm.com.cn